Structural, Magnetic, Dielectric, and Ferroelectric Properties of CoFe$_2$O$_4$-BaTiO$_3$ Nanocomposites

Nidhi Sheoran[1] · Sourabh Sharma[2] · Mukesh Sheoran[3] · Vinod Kumar[2] · Ashok Kumar[1] · O. P. Thakur[2]

Abstract

Nano-size spinel ferrite CoFe$_2$O$_4$ (CFO), ferroelectric BaTiO$_3$ (BTO), and their nanocomposites BTO@CFO (BTO nanoparticles are added during the synthesis of CFO) and CFO@BTO (CFO nanoparticles are added during the synthesis of BTO) were synthesized using a combination of chemical co-precipitation and sol–gel routes, respectively. The phase formation and crystallinity of the bare CFO and BTO and their nanocomposites were verified via x-ray diffraction (XRD) patterns. High-resolution transmission electron microscopy (HRTEM) revealed the formation of the nanocomposites. Magnetization measurements confirmed the ferromagnetic behavior of all the samples except BTO, in which superposition of a weak ferromagnetic and diamagnetic response occurred due to its nanostructure. Magnetization versus temperature (*M–T* plot) measurements showed an anomaly near the ferroelectric-to-paraelectric phase transition of BTO. Also, the dielectric constant (ε') and loss tangent (tanδ) with respect to frequency (10^2–10^6 Hz) and temperature (300–700 K) were examined. The ε'–*T* curve of the nanocomposites exhibited an anomaly at the same temperature as observed in the *M–T* plot, indicating the inherent magnetoelectric coupling in the nanocomposites. The energy storage properties of BTO and the nanocomposites were examined via *P–E* loop analysis and confirmed that the CFO@BTO sample exhibits maximum energy storage efficiency.

Keywords Nanocomposites · ferroelectric · ferromagnetic · perovskites

Introduction

Multiferroic materials perform an important role in the development of multifunctional devices that simultaneously show ferroelectric, ferromagnetic, and piezo-elastic order in the same phase.[1,2] Materials revealing spontaneous magnetization due to spontaneous polarization by a large coupling interaction could make it possible to control an electric field using a magnetic field, and vice versa.[3] This is the consequence of the magnetoelectric phenomenon. These multiferroic materials have garnered considerable interest within the scientific community because of their possible applications in multifunctional devices such as memory elements with multiple states, transducers, spintronics, and sensors, and terahertz radiation applications.[1,4] As a result of the mutual exclusivity of ferroelectricity and ferromagnetic arrangements, single-phase multiferroic materials such as BiFeO$_3$, BiMnO$_3$, and YMnO$_3$ are relatively rare.[1] Additionally, the magnetic response, dielectric constant, and magnetic permeability of single-phase multiferroics are restricted by phenomenological theory.[5] Therefore, the production of single-phase multiferroic compounds having high magnetoelectric coupling for use as multifunctional devices is challenging.[6] In the last two decades, much effort has been focused on resolving the issues with single-phase multiferroic materials. Earlier studies show that a composite of multiphase multiferroics possesses higher magnetoelectric (ME) coupling coefficients with larger values of magnetization and polarization than single-phase multiferroic materials.[7–9] ME

✉ Sourabh Sharma
saurabh.sharma2138@gmail.com

✉ Ashok Kumar
ashokkumar.phy@dcrustm.org

1 Department of Physics, Deenbandhu Chhotu Ram University of Science and Technology, Murthal, Haryana 131039, India

2 Materials Analysis and Research Laboratory, Department of Physics, Netaji Subhas University of Technology, New Delhi 110078, India

3 Department of Physics, Govt. College, Barota, Sonipat, Haryana 131301, India

coupling in composites occurs at the boundary of magnetic and ferroelectric phases. Nanocomposites offer an interesting and effective technique for novelty in functioning materials. However, the synthesis mechanism of nanocomposites has several disadvantages, including differences in thermal expansion, grain boundaries, and discrepancies between crystal parameters. Thus, to eliminate these problems, nanocomposites consisting of ferromagnetic and ferroelectric materials could offer a solution. The synergistic effect of nanocomposites provides modified properties, making them highly functional materials.[10] Although various research has been reported on the nanocomposites of $CoFe_2O_4/BaTiO_3$, $CoFe_2O_4/BiFeO_3$, and $NiFe_2O_4/BiFeO_3$,[11–13] there is still a lack of systematic reports on the development of uniform nanocomposites of multiferroic materials. Nanocomposites having very strong interactions should be (a) a medium that transfers strain ideally, (b) a dielectric layer that reduces the leakage problem by decreasing the conductivity of composites, and (c) able to provide enhanced magnetoelectric coupling.[14,15] $BaTiO_3/CoFe_2O_4$ composites possess better magnetoelectric properties as a result of individual phase contributions. Perovskite $BaTiO_3$ (BTO) is an excellent, efficient ceramic with interesting ferroelectric and optical properties, making it suitable for applications such as multilayer ceramic capacitors (MLCC), converters, actuators, and random access ferroelectric memory devices with energy storage applications.[16] $BaTiO_3$ mainly exhibits ferroelectric properties, but it can be multiferroic if it is synthesized at the nanoscale. Thus, in the present work, we explore the multiferroic properties of $BaTiO_3$ by synthesizing it via the sol–gel method to develop nanoparticles of $BaTiO_3$. Spinel ferrite $CoFe_2O_4$ (CFO) possesses outstanding electrical, magnetic, and optical properties, especially on a nanometer scale. Thus, we explore the multifunctional properties of CFO@BTO and BTO@CFO nanocomposites by studying their structural, magnetic, dielectric, and energy storage properties.

Experimental

Synthesis of BTO Nanoparticles and CFO@BTO Nanocomposite

BTO nanoparticles were synthesized via the sol–gel technique. Firstly, barium carbonate (1.9 g) was dissolved in 10 ml ethanol with continuous stirring for 30 min at room temperature. In parallel, titanium tetra isopropoxide (2.8 ml) was separately dissolved in 10 ml ethanol with continuous heating (353 K) and stirring on a hot plate for 30 min. These two solutions were then mixed in a single beaker with continuous stirring for 20 min. After that, citric acid (4.20 g) was added to the mixed solution followed by continuous

stirring and heating at 353 K for 30 min. Finally, a thick white gel was formed. The gel was further dried in an oven at 393 K for 2 h and then annealed at 873 K and 1073 K for 2 h in a programmable muffle furnace to obtain barium titanate powder. This powder was crushed in a mortar and pestle to obtain fine nanoparticles of BTO. In addition, CFO@BTO nanocomposites in a 1:1 weight ratio of CFO and BTO were synthesized by following the same steps as for BTO except for one additional step in which already synthesized CFO nanoparticles were added near the step of gel formation. The synthesis steps for the CFO nanoparticles are given in the following section. Finally, the obtained nanocomposites were annealed at 1073 K.

Synthesis of CFO and BTO@CFO Nanocomposite

CFO nanoparticles were prepared by chemical co-precipitation. Cobalt nitrate $Co(NO_3)_2 \cdot 6H_2O$ (6.39 g) and iron nitrate $Fe(NO_3)_3 \cdot 9H_2O$ (17.57 g) were dissolved in 60 ml of distilled water and stirred for 30 min in order to obtain a homogeneous solution. Oleic acid (10 ml) was added as a surfactant to prevent the agglomeration of the particles, followed by stirring for about 30 min at 353 K. After that, the precipitating agent liquid NH_3 was added dropwise under constant stirring to obtain a solution pH equal to 9. The precipitate was finally dried at 373 K on a hot plate and crushed by an agate mortar to obtain the nanoparticles. The CFO nanoparticles were then annealed at 1073 K for 2 h. The synthesis steps for the BTO@CFO nanocomposite at a 1:1 weight ratio of BTO and CFO were the same as the steps for the CFO nanoparticles except for one additional step, in which BTO nanoparticles were added before the precipitation step. Finally, the obtained nanocomposites were annealed at 1073 K.

Instrumentation Specifications

A Rigaku Ultima IV powder x-ray diffractometer with CuK_α radiation was used for structural and phase analysis of the developed samples. High-resolution transmission electron microscopy (HRTEM; FEI Tecnai G2 20, S-Twin) was employed to identify the core–shell nanostructure. A vibrating-sample magnetometer (Lake Shore Series 7410) with a magnetic field range ± 2 T was used for room-temperature and temperature-dependent magnetization measurements. For temperature-dependent measurements, a constant magnetic field of 500 Oe and a temperature range of 300–800 K were used. An impedance analyzer with a frequency range of 100 Hz to 1 MHz (Wayne Kerr 6500B) was used for dielectric measurements. Ferroelectric measurements were carried out using a P–E loop tracer (Marine India) at room temperature.

Results and Discussion

XRD Analysis

The x-ray diffraction (XRD) patterns of BTO synthesized at different annealing temperatures are shown in Fig. 1. BTO1 represents the raw sample without annealing, and BTO2 and BTO3 represent the BTO powder samples annealed at 873 K and 1073 K, respectively. The XRD results show that BTO1 has very low crystallinity, and phases do not grow at this temperature. At an annealing temperature of 873 K, the BTO phases appear with extra peaks due to residual BaCO$_3$ material. The reason for the presence of residual BaCO$_3$ peaks is the incomplete reaction between the precursors to form BTO.

These BaCO$_3$ phases of orthorhombic structure are identified by ICSD file number 91888. Finally, the pure phase of BTO with fine crystallinity was obtained after annealing at a temperature of 1073 K. At this temperature, the intensity of the BTO phase was enhanced and all the extra peaks of residual BaCO$_3$ disappeared. The peaks of the perovskite BTO phase with a tetragonal structure are identified as ICSD file number 29148.

Figure 2 presents the XRD patterns of bare CFO, BTO, and their nanocomposites CFO@BTO and BTO@CFO. The XRD patterns of both nanocomposites clearly show characteristic peaks of both ferrite (CFO) and ferroelectric (BTO) phases. The peaks of nanocomposites are indexed as shown in Fig. 2, which matches the peak location and intensities recorded in the ICSD data file for the CFO and BTO phase. Also, no undesired extra impurity phases are detected in the
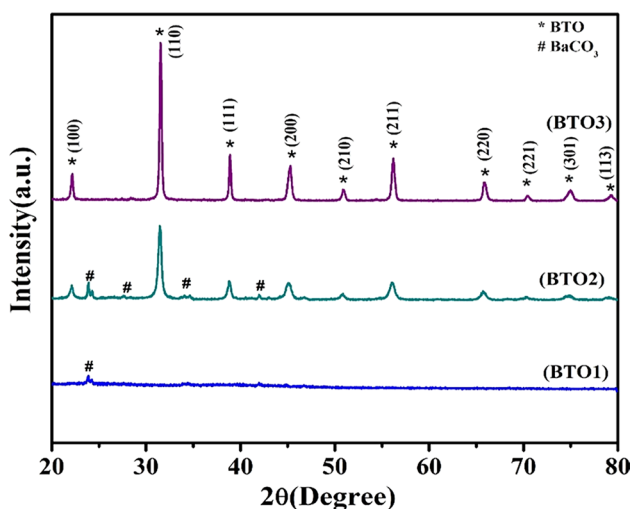
XRD pattern, indicating the absence of a chemical reaction between these two phases.

The lattice parameter values calculated for the BTO and CFO phases are tabulated in Table I. These lattice parameters closely match with previous results.[17,18] The average crystallite size (D) was calculated by the Debye–Scherrer equation,

$$D = \frac{k\lambda}{\beta \cos \theta}, \tag{1}$$

where k is the shape factor, with a value of 0.89, λ represents the x-ray wavelength, the peak position is determined by θ, and β is the full width at half maximum for the maximum intensity peak.

Microscopy Analysis

HRTEM micrographs of the BTO nanoparticles and CFO@BTO nanocomposite are shown in Fig. 3a and b, respectively. The magnified view of the CFO@BTO nanocomposite is
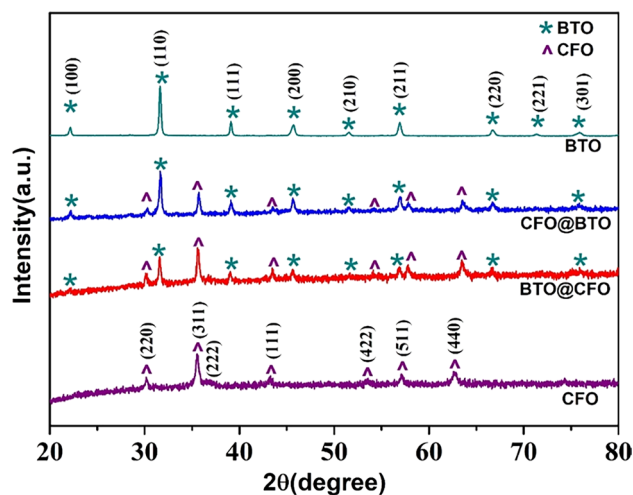
Fig. 2 XRD pattern of CFO, BTO@CFO, CFO@BTO, and BTO. The symbols * and ^ represent the BTO and CFO phases, respectively.

Table 1 Lattice parameters and crystallite size of CFO, BTO@CFO, CFO@BTO, and BTO nanoparticles

Sample	Lattice parameters (Å)			Crystallite size, D (nm)	
	CFO a (Å)	BTO		CFO	BTO
		a=b (Å)	c (Å)		
CFO	8.382	–	–	29	–
BTO@CFO	8.349	3.993	3.991	32	38
CFO@BTO	8.333	3.995	3.998	34	37
BTO	–	3.999	4.010	–	39

Fig. 1 XRD pattern of BTO nanoparticles at different annealing temperatures, designated as BTO1 (without annealing), BTO2 (873 K), and BTO3 (1073 K).
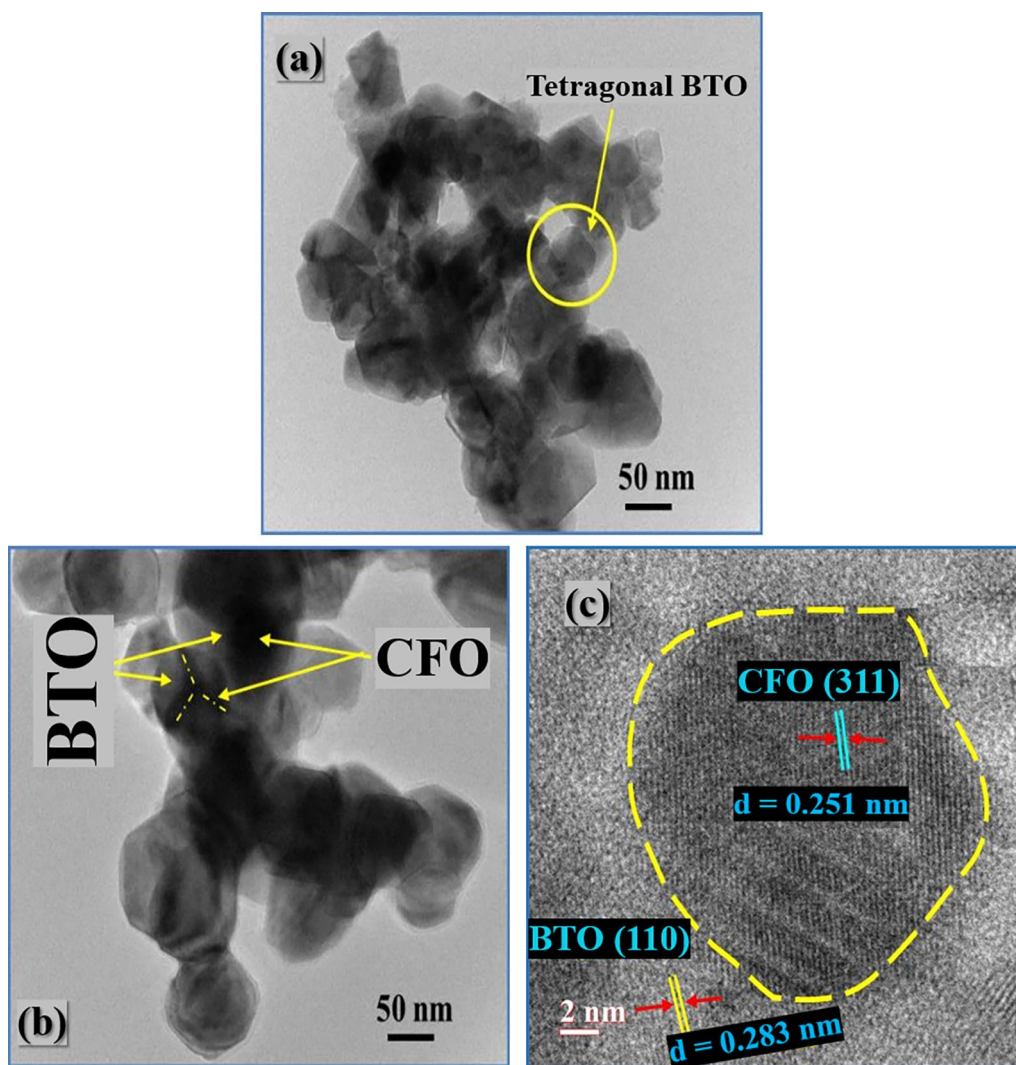
Fig. 3 HRTEM micrograph of (a) BTO, (b) CFO@BTO, (c) magnified view of CFO@BTO representing d spacing of individual phases.

depicted in Fig. 3c. Figure 3a clearly shows tetragonal BTO nanoparticles with particle size $\sim$49 nm, determined by the XRD results. Figure 3b and c present the formation of the CFO@BTO nanocomposite as a result of the difference in transmission intensity between the BTO and CFO phases. BTO and CFO are identified in the HRTEM micrographs by the measured value of lattice spacing $d = 0.251$ nm in the dark region, which corresponds to the CFO phase, and $d = 0.283$ nm in the bright region, which corresponds to the BTO phase. Further, from Fig. 3b, the measured diameter of CFO is $\sim$50 nm and that of BTO is $\sim$17.5 nm. Magnetic CFO nanoparticles form agglomerates in the BTO matrix.

Figure 4a shows the HRTEM micrograph of the BTO@CFO nanocomposite with the presence of some agglomerates and an arbitrary mixture of BTO and CFO phases. Figure 4b shows the magnified view of this nanocomposite which reveals an interplanar distance $d = 0.252$ nm of the

BTO phase and $d = 0.282$ nm of the CFO phase. In Fig. 4a, the magnetic CFO nanoparticles form agglomerates around the BTO matrix, and the average particle size of the BTO@CFO nanocomposite is 56 nm.

Magnetic Analysis

The M–H curve of the BTO nanoparticles exhibits superposition of diamagnetic and weak ferromagnetic contributions, as shown in Fig. 5a. The variation in magnetization M in the vicinity of $\pm H_c$ ($H_c \sim 830$ Oe is the coercive field strength) represents weak ferromagnetic behavior. The M–H plot without diamagnetic contribution is shown in Fig. 5b. The observed value of spontaneous magnetization (0.003 emu/g) is similar to that in previously reported results.[19] Such behavior in BTO nanoparticles is attributed to the presence of defects such as oxygen vacancies on the
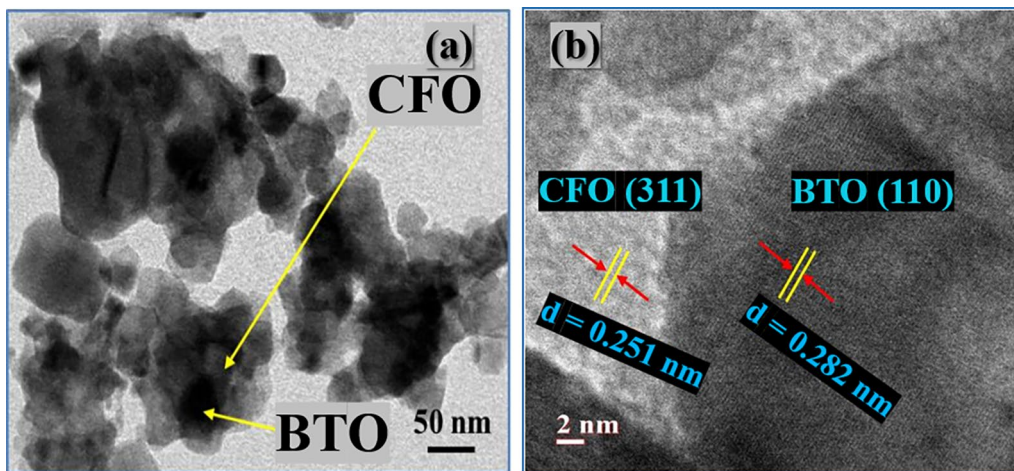
Fig. 4 HRTEM micrograph of (a) BTO@CFO, (b) magnified view of BTO@CFO representing *d* spacing of individual phases.

surface of the grains. These oxygen vacancies at the surface generate Ti^{3+}-O in the interstitial position and Ti^{3+}-V_o at the surface, where V_o is a void due to oxygen deficiency.[20]

In Fig. 6, the *M*–*H* loops of CFO, CFO@BTO, and BTO@CFO exhibit hysteresis and show ferromagnetic behavior. The saturation magnetization (M_s), remnant magnetization (M_r), coercivity (H_c), anisotropy constant (K), and squareness ratio (*S*) values are tabulated in Table II. Both nanocomposites exhibit a smaller value of magnetization than CFO nanoparticles. The magnetic moments in the nanocomposites arise mostly due to CFO nanoparticles, as BTO exhibits very little magnetization. CFO@BTO has a slightly higher magnetization value than BTO@CFO. Two types of magnetic interaction occur in the composite samples: the superexchange interaction within CFO nanoparticles and the exchange interaction at the interface of BTO and CFO phases.

To establish the domain structure of the CFO phase and composites, the squareness ratio (*S*) was estimated, as shown in Table II. The observed values of *S* indicate that both the CFO phase and nanocomposites are multidomain-structured ($S < 0.5$).[21] To investigate the magnetic transition temperature (T_c) of the CFO, CFO@BTO, and BTO@CFO nanoparticles, *M*–*T* plots with an applied magnetic field of 500 Oe are displayed in Fig. 7a, b, and c, respectively. Figure 7a shows that at low temperatures, there is a small variation in magnetization, whereas a dramatic variation occurs at high temperatures. This sharp decrease in magnetization at high temperatures is attributable to the disappearance of ferrimagnetic behavior above the magnetic transition temperature T_c (= 734 K) for pure CFO nanoparticles. Figure 8b and c show this magnetic transition temperature at T_c = 653 K and T_c = 610 K for the CFO@BTO and BTO@CFO nanocomposites, respectively. It has been found that the magnetic moment decreases with increasing temperature, causing a phase transition from ferrimagnetism to paramagnetism. This is due to the increased thermal randomization of the magnetic moment at increased temperature.[22,23]

When heating is applied with an applied magnetic field, the magnetic arrangement in CFO nanoparticles is constantly transformed from a canted to a collinear state, which leads to an increase in magnetization. However, it has been shown that T_c values in nanocomposites are slightly reduced relative to pure CFO. This decrease in the T_c values for the nanocomposites is due to the diffusion of the BTO into the spinel lattice, which weakens the superexchange interaction.[24] This weakening of the superexchange interaction is the result of an increase in the separation of magnetic moments at the A and B positions of the spinel structure. Weak superexchange interactions are more easily affected by the thermal motion, which results in the lower T_c of the nanocomposites. In Fig. 7a and c, *M*–*T* measurements show the magnetic anomaly at 362 K and 349 K, respectively. This magnetic anomaly in both nanocomposites shows the ferroelectric phase transition of BTO, as these anomalies lie near the standard ferroelectric ~ 390 K of BTO. Also, the increase in magnetization near the phase transition temperature of BTO in both nanocomposites may be due to a sharp increase in compressive strain.[25] Thus, these anomalies indicate the magnetoelectric coupling effect in both nanocomposites.

Dielectric Analysis

Figure 8a and b depict the change in the dielectric constant (ε') and loss tangent (tanδ), respectively, in the frequency range 10^2–10^6 Hz for all the samples. The dielectric constant of all samples exhibits a strong frequency dependence, with a larger value at low frequencies and decreasing with increasing frequency, attaining the continual behavior like a typical dielectric. The largest dielectric constant value
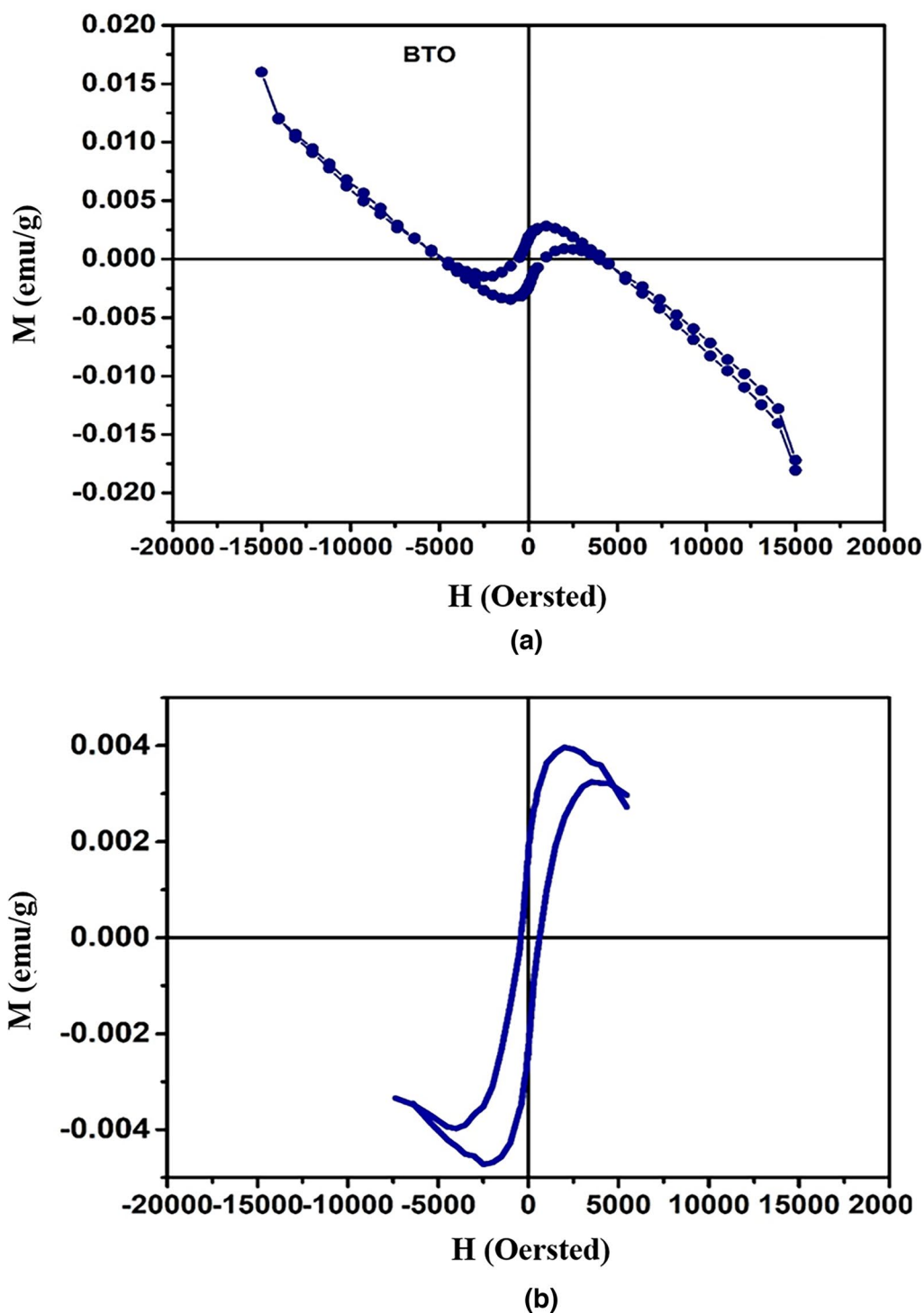
Fig. 5 (a) *M–H* plot for BTO nanoparticles and (b) *M–H* curve obtained after excluding the diamagnetic contribution from the *M–H* plot of BTO.

at a small frequency region may be demonstrated on the grounds of charge polarization by a nonhomogeneous dielectric structure and Maxwell–Wagner space charge polarization, in accordance with Koop's phenomenological theory. These models play a major role in such types of multiphase composites.[26–30] In this model, the dielectric structure of the ferrite and composites was supposed to consist of highly conductive layers of grains surrounded by weakly conducting grain boundaries. At small frequencies, greater polarization occurs due to the active participation of the grain

boundary and its fast response to the applied field. Therefore, greater charge accumulation takes place at the grain boundary interface, which results in a high dielectric constant. In the lower-frequency region, the electric dipole is in phase with the applied field frequency, but in the higher-frequency region, these dipoles are unable to keep pace with the fast changes in the applied field. Thus, CFO@BTO exhibits a higher dielectric constant than BTO@CFO due to its in situ composite formation in which there is an ordered arrangement of ferroelectric and ferrite layers. In BTO@CFO, however, due to the agglomeration of CFO nanoparticles around BTO, large conducting channel formation takes place that decreases the value of the dielectric constant. The tanδ value represents the tangent loss in the sample, which measures the electrical energy loss due to the applied electric field at various frequencies. The nanocomposites exhibit smaller tangent loss values than the BTO and CFO phase. Therefore, these nanocomposites are useful for high-frequency microwave devices.

The distinct trends observed in the imaginary part of the dielectric constant (ε'') highlight the interplay between the dielectric and magnetic properties in these materials. The higher value of BTO at low frequencies indicates strong polarization, while the lower value in CFO reflects minimal dipolar contributions. The nanocomposites exhibit
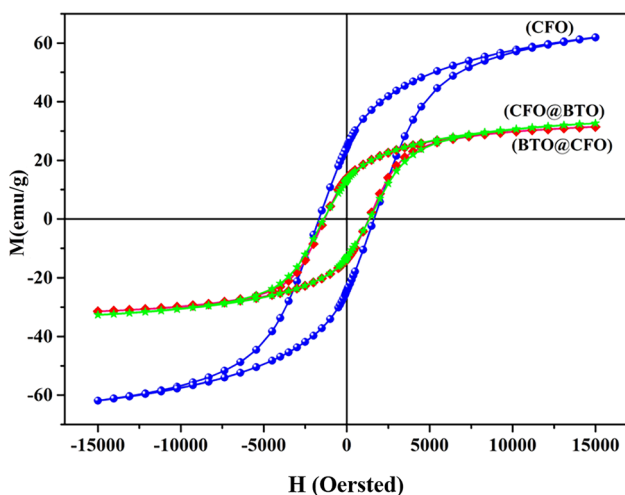

Fig. 6 Room-temperature *M–H* loops of CFO, CFO@BTO, and BTO@CFO nanoparticles

intermediate behaviors, with the configuration of BTO and CFO significantly influencing the dielectric properties. These findings are crucial for the design and application of these materials in electronic devices. For instance, the high ε'' value of BTO at low frequencies can be advantageous in applications requiring high energy dissipation, such as capacitors. Conversely, the low ε'' value of CFO and the tailored properties of the nanocomposites make them suitable for applications such as high-frequency inductors and transformers.

Figure 9 displays the change in the dielectric constant with respect to the temperature of the nanocomposites and BTO (inset) at a frequency of 10 kHz. The dielectric constant increases up to the first transition temperature range of 350–370 K, and then it reaches a second maximum and then decreases again. The increase in the dielectric constant with temperature is attributed to interfacial polarization at the ferrite/ferroelectric boundary and also due to the hopping conduction mechanism, which is a process of thermal activation.[27] The first anomaly in the temperature range 350–370 K corresponds to the ferroelectric phase transition of the BTO phase, which suggests the presence of a ferroelectric phase in these nanocomposites. Another peak in the temperature range of 640–680 K is attributed to the transition in the dielectric constant close to the T_c of the CFO phase.[8]

Near the transition temperature, large dielectric constants are attributed to the effect of temperature change on domain wall motion. At lower temperatures, the domain wall contributes to a small dielectric constant because of difficulties in the movement of domains.[31] However, at the transition temperature, the high dielectric constant value is attributed to domain wall motion, and beyond the transition temperature, it decreases due to difficulty in the orientation of domains in the path of a functional electric field.[32] The Curie temperature of BTO is ~ 390 K. But here we observed a decrease in the Curie temperature (T_c) for both BTO nanoparticles and nanocomposites, which can be attributed to the intrinsic size effect, because the nano-sized (< 100 nm) BTO induces stress inside the grain, thereby inhibiting the movement of the domain wall. Thus, the competition between the shrinkage of surface bonds and the pinning of domain walls affects the phase transition of the BTO.[33] The *M–T* plot of the nanocomposite exhibits an anomaly at the same

Table II Saturation magnetization (M_s), remnant magnetization (M_r) coercivity (H_c), *S* (squareness ratio), and T_c (Curie temperature) of CFO, CFO@BTO, and BTO@CFO nanocomposites

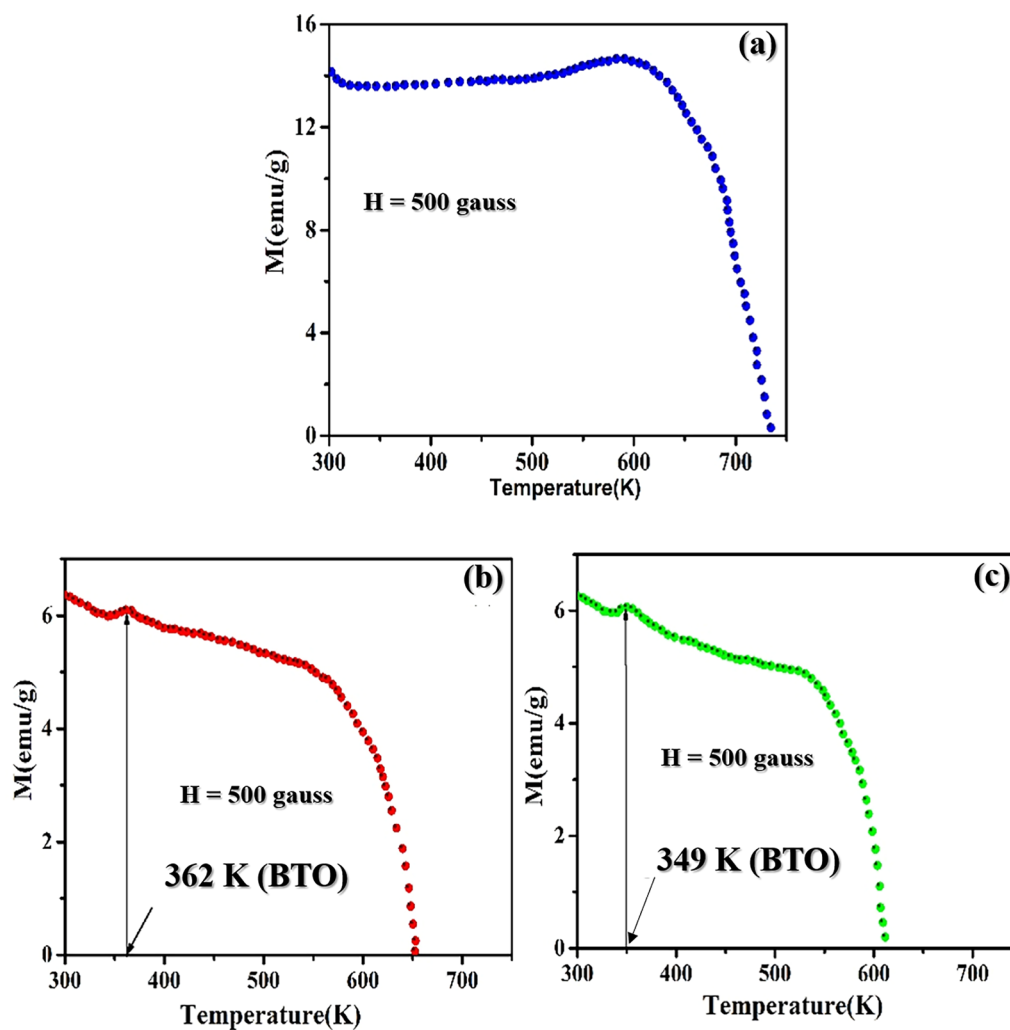| Samples	M_s (emu/g)	M_r (emu/g)	H_c (Oe)	$S = M_r/M_s$	$K = H_c M_s/M$	T_c (K)	
						BTO	CFO
CFO	62.25	26.72	1687	0.43	447.60	–	734
CFO@BTO	32.61	13.74	1402	0.42	97.73	362	653
BTO@CFO	31.33	14.04	1351	0.44	90.47	349	610

Fig. 7 Magnetization versus temperature (*M–T*) plot at applied magnetic field of 500 Oe for (a) CFO, (b) CFO@/BTO, and (c) BTO@CFO nanoparticles.
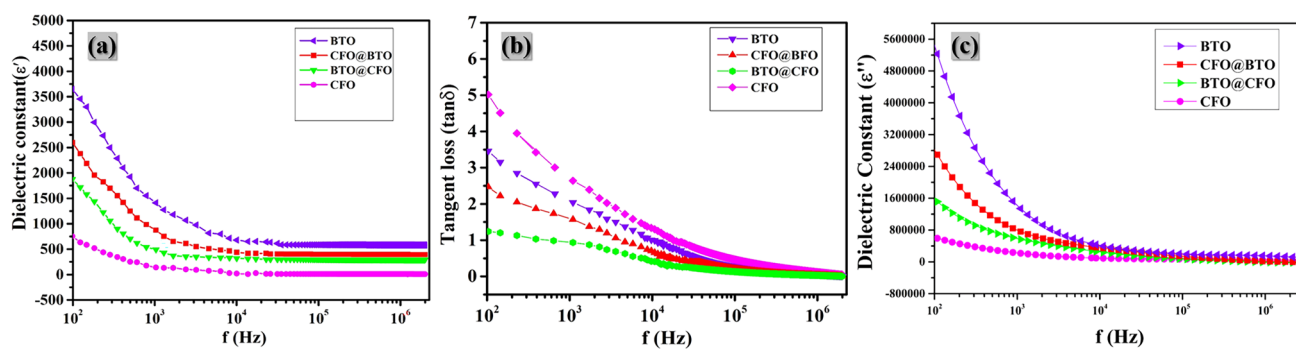

Fig. 8 Frequency-dependent behavior for (a) dielectric constant (ε'), (b) tangent loss, and (c) dielectric constant (ε'') of BTO, CFO, CFO@BTO, and BTO@CFO nanoparticles at room temperature.
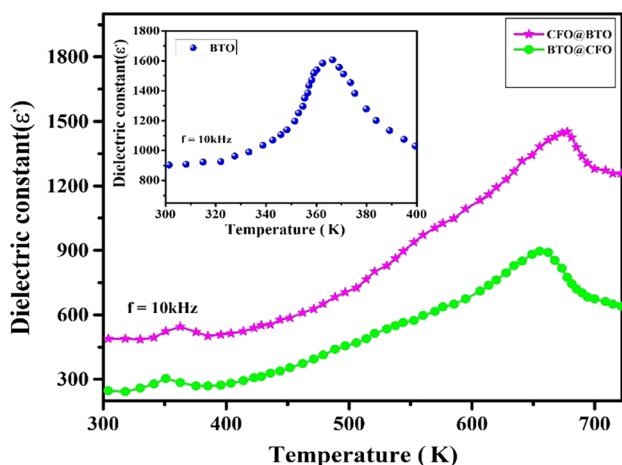
Fig. 9 Temperature-dependent dielectric constant of BTO (inset), CFO@BTO, and BTO@CFO nanoparticles at a fixed frequency of 10 kHz.
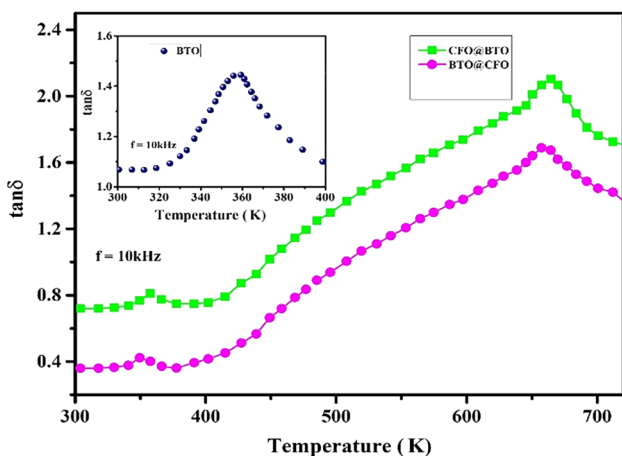

Fig. 10 Temperature-dependent tanδ (tangent loss) of BTO (inset) and CFO@BTO and BTO@CFO nanocomposites at a fixed frequency of 10 kHz.

temperature, indicating the intrinsic magnetoelectric coupling in both nanocomposites.

Figure 10 displays a change in tangent loss with respect to temperature at a frequency of 10 kHz, and it exhibits the same behavior as that observed for the dielectric constant variation in Fig. 10. The increase in tanδ with temperature may be attributed to the thermally activated conduction mechanism.[34] At high temperatures, the substantial increase in the tanδ of the composites is attributed to interfacial polarization at the CFO@BTO interface and enhanced thermally stimulated dielectric relaxation.[35]

Ferroelectric Analysis

Figure 11 displays the *P–E* hysteresis loop at a frequency of 50 Hz for all the samples. BTO and the nanocomposites exhibit typical ferroelectric behavior. The values of maximum polarization (P_m), remnant polarization (P_r), and coercivity (E_c) are tabulated in Table III. The CFO@BTO sample exhibits the highest maximum polarization (P_m) at an applied electric field of 15 kV/cm, which can be attributed to the large number of space polarizations that occur across the long chain of ordered ferrite/ferroelectric phases.

BTO exhibits a small P_m value because ferroelectric behavior may be reduced in nano-sized BTO particles due to the increased oxygen vacancies. The *P–E* loop is used to evaluate the energy storage density and storage efficiency of all samples. The energy storage density (W_U) and efficiency (η) can be calculated using the following relations[15,16]:

$$W_U = \int_0^{P_{max}} E \cdot dP, \tag{2}$$

$$\eta = \frac{W_U}{W_U + W_L}, \tag{3}$$

where *E* and *P* represent the applied electric field and polarization, respectively, and W_U and W_L are energy storage density and energy loss density, respectively. The gray region in the *P–E* loops shows the losses, and the orange region shows the recoverable useful energy. CFO@BTO exhibits higher efficiency than other samples, as depicted in Table III. Therefore, these composite samples can be used for storage capacitor devices.[36–38]

Conclusion

BTO, CFO, and their nanocomposites CFO@BTO and BTO@CFO were synthesized by the sol–gel and co-precipitation methods. XRD analysis confirmed that all respective phases were present in the bare and nanocomposite samples. HRTEM confirmed the nanocomposites and nano-size of the developed materials. The *M–H* hysteresis curve showed the typical ferromagnetic behavior of CFO and nanocomposites, and weak ferromagnetism was observed in the BTO sample around $\pm H_c \sim 830$ Oe (excluding the diamagnetic part) due to its nano-size effect. CFO@BTO has a larger value of magnetization and Curie temperature than the BTO@CFO nanocomposite. The large value of the dielectric constant in low-frequency regions was attributed to the origin of space charges and the hopping mechanism of charge carrier conduction. The dielectric constant versus temperature curve explained the presence of magnetoelectric coupling in
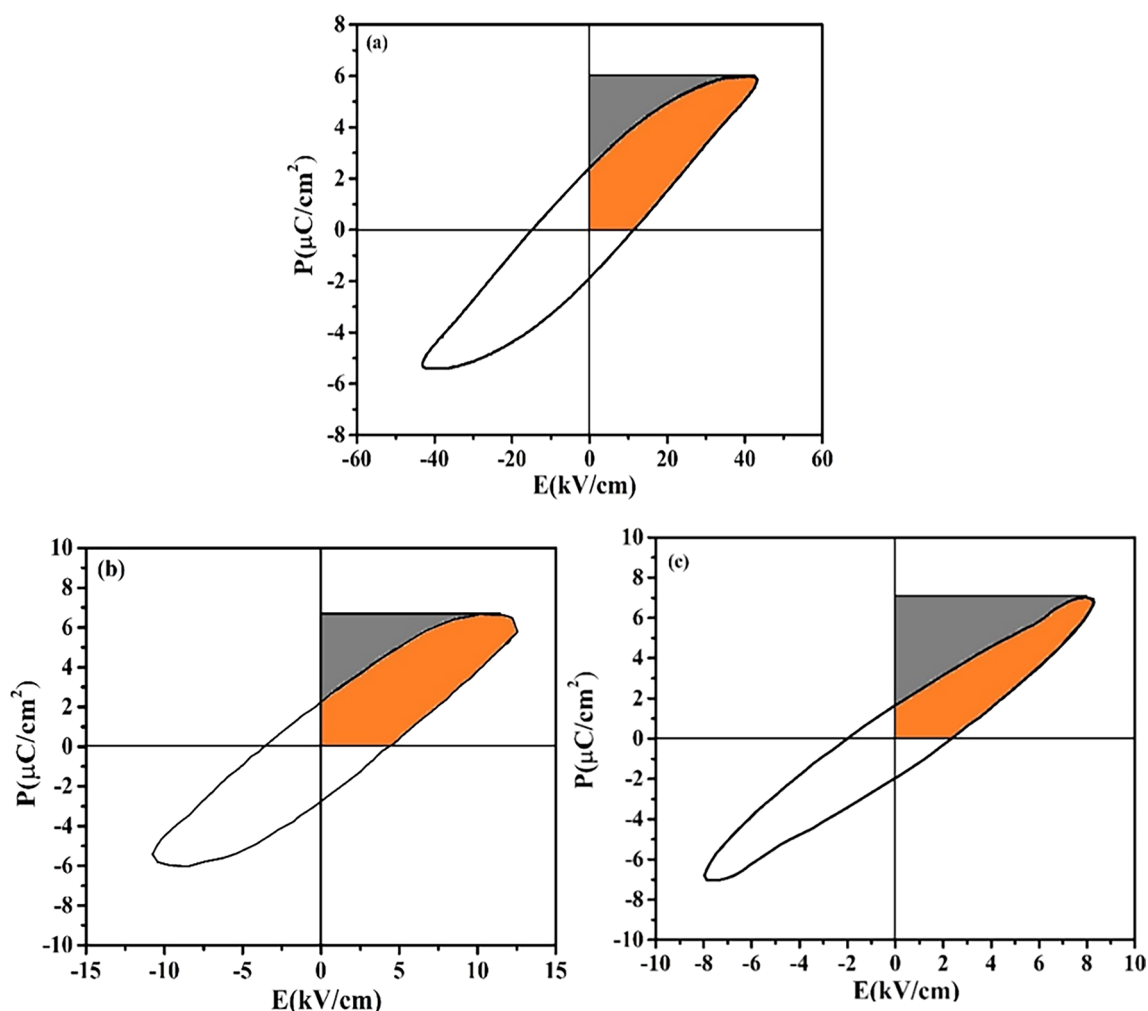
Fig. 11 *P–E* loop behavior of BTO, CFO@BTO, BTO@CFO, and CFO nanoparticles at room temperature.

Table III Maximum polarization (P_m), remnant polarization (P_r), coercivity (E_c), energy storage density (W_U), and energy storage efficiency (η) of all samples

Sample	P_m (µC/cm^2)	P_r (µC/cm^2)	E_c (kV/cm)	W_U (mJ/cm^3)	η (%)
BTO	5.96	2.39	11.168	102.31	62.10
CFO@BTO	6.65	2.19	4.54	36.97	64.06
BTO@CFO	7.01	1.66	2.33	19.49	48.01

composite samples based on anomalies present in the curve. *P–E* loop analysis examined the energy storage efficiency of all the samples and showed that CFO@BTO exhibited maximum energy storage efficiency, at 64%. The nanocomposites of the ferrite (CFO)/ferroelectric (BTO) phase will be useful for storage and multistate memory devices.

References

1. W. Eerenstein, N.D. Mathur, and J.F. Scott, Multiferroic and magnetoelectric materials. *Nature* 442, 759 (2006).
2. N.A. Spaldin and R. Ramesh, Advances in magnetoelectric multiferroics. *Nat. Mater.* 18, 203 (2019).
3. P. Kumar and P. Chand, Large electric field driven strain and enhanced multiferroic properties of Ce^{3+}/BiFeO$_3$ Nano photocatalyst. *Mater. Sci. Semicond. Process.* 144, 106576 (2022).
4. B. Raneesh, H. Soumya, J. Philip, S. Thomas, and K. Nandakumar, Magnetoelectric properties of multiferroic composites (1–x)ErMnO3–xY3Fe5O12 at room temperature. *J. Alloy. Compd.* 611, 381 (2014).

5. Y. Liu, Y. Wu, D. Li, Y. Zhang, J. Zhang, and J. Yang, A study of structural, ferroelectric, ferromagnetic, dielectric properties of NiFe$_2$O$_4$–BaTiO$_3$ multiferroic composites. *J. Mater. Sci. Mater. Electron.* 24, 1900 (2013).

6. P. Jain, S. Shankar, and O.P. Thakur, Unveiling the impact of Ni^{2+}/Y^{3+} co-substitution on the structural, dielectric, and impedance properties of multiferroic spinel ferrite for hydroelectric cell application. *Phys. Chem. Chem. Phys.* 25, 21280 (2023).

7. D.K. Pradhan, R.N.P. Chowdhury, and T.K. Nath, Magnetoelectric properties of PbZr$_{0.53}$Ti$_{0.47}$O$_3$–Ni$_{0.65}$Zn$_{0.35}$Fe$_2$O$_4$ multiferroic nanocomposites. *Appl. Nanosci.* 2, 261 (2012).

8. D.P. Dutta, B.P. Mandal, R. Naik, G. Lawes, and A.K. Tyagi, Magnetic, ferroelectric, and magnetocapacitive properties of sonochemically synthesized Sc- doped BiFeO$_3$ nanoparticles. *J. Phys. Chem. C* 117, 2382 (2013).

9. K.S. Kumar, S. Ramu, A. Sudharani, M. Ramanadha, G. Murali, and R.P. Vijayalakshmi, Enhanced magnetic and dielectric properties of Gd doped BiFeO$_3$: Er nanoparticles synthesized by sol-gel technique. *Phys. E Low Dimens. Syst. Nanostruct.* 115, 113689 (2020).

10. F. Li, M. Zeng, H. Yu, H. Xu, and J. Li, Dielectric characteristics of B-site-modified hexagonal-barium titanate. *J. Mater. Sci. Mater. Electron.* 27, 2836 (2016).

11. C.A. Vaz, J. Hoffman, C.H. Ahn, and R. Ramesh, Magnetoelectric coupling effects in multiferroic complex oxide composite structures. *Adv. Mater.* 22, 2900 (2010).

12. A.K. Sahu, P. Mallick, S.K. Satpathy, and B. Behera, Effect on structural, electrical and temperature sensing behavior of neodymium doped bismuth ferrite. *Adv. Mater. Lett.* 12, 1 (2021).

13. G. Allaedini, S.M. Tasirin, and P. Aminayi, Magnetic properties of cobalt ferrite synthesized by hydrothermal method. *Int. Nano Lett.* 5, 183 (2015).

14. M. Chandrasekhar and P. Kumar, Synthesis and characterizations of NaNbO$_3$ modified BNT–BT–BKT ceramics for energy storage applications. *Phys. B Condens. Matter* 497, 59 (2016).

15. M. Chandrasekhar and P. Kumar, Synthesis and characterizations of BNT–BT and BNT–BT–KNN ceramics for actuator and energy storage applications. *Ceram. Int.* 41, 5574 (2015).

16. V.S. Puli, D.K. Pradhan, B.C. Riggs, D.B. Chrisey, and R.S. Katiyar, Investigations on structure, ferroelectric, piezoelectric and energy storage properties of barium calcium titanate (BCT) ceramics. *J. Alloy. Compd.* 584, 369 (2014).

17. V. Corral-Flores, D. Bueno-Baques, and R.D. Ziolo, Synthesis and characterization of novel CoFe$_2$O$_4$–BaTiO$_3$ multiferroic core–shell-type nanostructures. *Acta Mater.* 58, 764 (2010).

18. E.V. Ramana, F. Figueiras, M.P.F. Graca, and M.A. Valente, Observation of magnetoelectric coupling and local piezoresponse in modified (Na0.5Bi0.5)TiO$_3$–BaTiO$_3$–CoFe$_2$O$_4$ lead-free composites. *Dalton Trans.* 43, 9934 (2014).

19. P. Zhang, D.S. Yang, T.D. Thanh, D.A. Tuan, and S.C. Yu, Origin of ferromagnetism in BaTiO$_3$ nanoparticles prepared by mechanical milling. *J. Appl. Phys.* 113, 17 (2013).

20. S. Qin, D. Liu, Z. Zuo, Y. Sang, X. Zhang, F. Zheng, and X.G. Xu, UV-irradiation- enhanced ferromagnetism in BaTiO$_3$. *J. Phys. Chem. Lett.* 1, 238 (2010).

21. A. Chaudhuri and K. Mandal, Large magnetoelectric properties in CoFe$_2$O$_4$: BaTiO$_3$ core–shell nanocomposites. *J. Magn. Magn. Mater.* 377, 441 (2015).

22. D. Pal, M. Mandal, A. Chaudhuri, B. Das, D. Sarkar, and K. Mandal, Micelles induced high coercivity in single domain cobalt-ferrite nanoparticles. *J. Appl. Phys.* 108, 12 (2010).

23. Z. Zi, Y. Sun, X. Zhu, Z. Yang, J. Dai, and W. Song, Synthesis and magnetic properties of CoFe$_2$O$_4$ ferrite nanoparticles. *J. Magn. Magn. Mater.* 321, 1251 (2009).

24. J.P. Zhou, L. Lv, Q. Liu, Y.X. Zhang, and P. Liu, Hydrothermal synthesis and properties of NiFe$_2$O$_4$@BaTiO$_3$ composites with well-matched interface. *Sci. Technol. Adv. Mater.* 13, 045001 (2012).

25. K.C. Verma, M. Singh, R.K. Kotnala, and N. Goyal, Magnetic field control of polarization/capacitance/voltage/resistance through lattice strain in BaTiO$_3$-CoFe$_2$O$_4$ multiferroic nanocomposite. *J. Magn. Magn. Mater.* 469, 483 (2019).

26. L. Sirdeshmukh, K. Krishna Kumar, S. Bal Laxman, A. Rama Krishna, and G. Sathaiah, Dielectric properties and electrical conduction in yttrium iron garnet (YIG). *Bull. Mater. Sci.* 21, 219 (1998).

27. Y.M. Xu and N. Zhang, Magnetocapacitance effects in MnZn ferrites. *AIP Adv.* 5, 11 (2015).

28. P.K. Jana, S. Sarkar, and B.K. Chaudhuri, Maxwell-Wagner polarization mechanism in potassium and titanium doped nickel oxide showing giant dielectric permittivity. *J. Phys. D Appl. Phys.* 40, 556 (2007).

29. A. Kumar and K.L. Yadav, Synthesis and characterization of MnFe$_2$O$_4$–BiFeO$_3$ multiferroic composites. *Phys. B Condens. Matter* 406, 1763 (2011).

30. C.G. Koops, On the dispersion of resistivity and dielectric constant of some semiconductors at audio frequencies. *Phys. Rev.* 83, 121 (1951).

31. B.K. Bammannavar, L.R. Naik, and B.K. Chougule, Studies on dielectric and magnetic properties of (x) Ni$_{0.2}$Co$_{0.8}$Fe$_2$O$_4$+(1−x) barium lead zirconate titanate magnetoelectric composites. *J. Appl. Phys.* 104, 6 (2008).

32. D.R. Patil, S.S. Chougule, S.A. Lokare, and B.K. Chougule, Electrical properties of xNiFe2O4+(1−x) Ba$_{0.7}$Sr$_{0.3}$TiO$_3$ composites. *J. Alloy. Compd.* 452, 414 (2008).

33. Z. Zhao, V. Buscaglia, M. Viviani, M.T. Buscaglia, L. Mitoseriu, A. Testino, and P. Nanni, Grain-size effects on the ferroelectric behavior of dense nanocrystalline BaTiO$_3$ ceramics. *Phys. Rev. B* 70, 024107 (2004).

34. A.S. Fawzi, A.D. Sheikh, and V.L. Mathe, Composition dependent electrical, dielectric, magnetic and magnetoelectric properties of (x) Co$_{0.5}$Zn$_{0.5}$Fe$_2$O$_4$+(1−x) PLZT composites. *J. Alloy. Compd.* 493, 601 (2010).

35. S. Basu, K.R. Babu, and R.N.P. Choudhary, Studies on the piezoelectric and magnetostrictive phase distribution in lead zirconate titanate–cobalt iron oxide composites. *Mater. Chem. Phys.* 132, 570 (2012).

36. S. Shankar, M. Kumar, V. Tuli, O.P. Thakur, and M. Jayasimhadri, Energy storage and magnetoelectric coupling in ferroelectric–ferrite composites. *J. Mater. Sci. Mater. Electron.* 29, 18352 (2018).

37. T. Wang, L. Jin, Y. Tian, L. Shu, Q. Hu, and X. Wei, Microstructure and ferroelectric properties of Nb$_2$O$_5$-modified BiFeO$_3$-BaTiO$_3$ lead-free ceramics for energy storage. *Mater. Lett.* 137, 79 (2014).

38. Q. Li, W. Zhang, C. Wang, L. Ning, Y. Wen, B. Hu, and H. Fan, Enhanced energy-storage performance of (1−x)(0.72 Bi$_{0.5}$Na$_{0.5}$TiO$_3$-0.28 Bi$_{0.2}$Sr$_{0.7\&0.1}$TiO$_3$)-xLa ceramics. *J. Alloy. Compd.* 775, 116 (2019).